Electron Transport Phenomena in Zinc at Liquid-Helium Temperatures*†

C. G. GRENIER, J. M. REYNOLDS, AND N. H. ZEBOUNI
Department of Physics, Louisiana State University, Baton Rouge, Louisiana
(Received 20 August 1962)

The magnetic-field dependences of the electrical and thermal resistances, the thermoelectric power, the Hall, the Righi-Leduc, the Peltier, the Ettingshausen, and the Ettingshausen-Nernst effects at liquid-helium temperatures in magnetic fields up to 14 kG, have been investigated in a single crystal of zinc. The measurements were taken with either a constant heat current or a constant electric current flowing perpendicular to the hexagonal axis and with the magnetic field parallel to the hexagonal axis. Original observations of de Haas–van Alphen type oscillations were made in the Righi-Leduc, the Peltier, and the Ettingshausen effects. Respective periods of 6.14, 6.28, and 6.45×10^{-5} G^{-1} were found. Like the Hall effect, the Righi-Leduc effect changes sign at about 5500 G. The Ettingshausen and the Peltier effects are strongly oscillatory with little monotonic variation with field. The oscillations in the Peltier effect and the thermal magnetoresistance exhibit a phase inversion near 5000 G similar to that in the Ettingshausen-Nernst effect and the magnetoresistance. This change in phase is correlated with the change in sign of the Hall and the Righi-Leduc effects at about the same field value. The longitudinal and transverse Lorenz ratios are equal and remain practically constant in high fields at a value of 2.35×10^{-8} V^2/deg^2, i.e., 4% smaller than the free-electron value. An extrapolated value of the lattice conductivity at 2°K is 0.02 W/deg-cm, i.e., about 0.02% of the zero-field electronic thermal conductivity. The thermoelectric effects are compared by means of the Onsager relations. Excellent agreement is found for the phase and amplitude of oscillations. The different kinetic coefficients relating fluxes to affinities were computed to facilitate comparison with theory. Curve fitting of the conductivity coefficients to Sondheimer-Wilson theory was attempted in terms of a four-band scheme. Analysis of the oscillations was attempted in terms of recent theory. The Righi-Leduc and the Hall conductivities, the Ettingshausen-Nernst, and the Ettingshausen effects (the transverse effects) strongly disagree with the expectation of any of the available theories, each exhibiting oscillations whose amplitude is several orders of magnitude larger than that calculated from any of the various theories. The results for the longitudinal effects (the thermal and the electrical conductivities, and the thermoelectric and the Peltier coefficients) are consistent, within the experimental error, with recent quantum-mechanical conductivity theories.

I. INTRODUCTION

THE oscillatory magnetic-field dependences of the magnetoresistance, Hall effect, thermoelectric power, and Ettingshausen-Nernst effect were studied in a single crystal of zinc by Bergeron, Grenier, and Reynolds.[1] In the course of their analysis, it became clear that any satisfactory comparison with theory would require a determination of all the components of the 6×6 tensor which relates the electrical and the thermal currents to the electric fields and the temperature gradients in the metal. Experiments on zinc from which these components are calculated are reported herein.

II. DEFINITIONS AND FUNDAMENTAL RELATIONS

The transport of an electric current density **J** and a heat current density **w** in a homogeneous isotropic conductor in the presence of a transverse magnetic field **H**, i.e., a magnetic field perpendicular to the direction of the currents, gives rise to a group of effects characterized by modifications of both an electric field **E** and a gradient of temperature, the negative of which is designated by **G**. The field vectors **E** and **G** are not parallel to the current vectors **J** and **w**. The different possible effects have been described by Callen[2] and Jan.[3] Those which have been measured in the present work are defined in Table I together with the conditions of their measurement. Linear relations can be established between the components of the field vectors and those of the current vectors. These relations can be written in various forms, depending both on the theoretical approach to the problem and on the particular experimental conditions.

TABLE I. Definition of the measured coefficients with conditions of measurement.

Name	Measured coefficients	Conditions
Isothermal electric resistivity	$\rho_{11}=E_1/J_1$	$J_2=G_1=G_2=0$
Isothermal Hall resistivity	$\rho_{21}=E_2/J_1$	$J_2=G_1=G_2=0$
Adiabatic thermal resistivity	$\gamma_{11}=G_1/w_1$	$J_1=J_2=w_2=w_2^*=0$
Adiabatic Righi-Leduc resistivity	$\gamma_{21}=G_2/w_1$	$J_1=J_2=w_2=w_2^*=0$
Adiabatic Peltier coefficient	$\pi_{11}'=G_1/J_1$	$J_2=w_1^*=w_2=w_2^*=0$
Adiabatic Ettingshausen coefficient	$\pi_{21}'=G_2/J_1$	$J_2=w_1^*=w_2=w_2^*=0$
Adiabatic thermoelectric coefficient	$\epsilon_{11}'=E_1^*/w_1$	$J_1=J_2=w_2=w_2^*=0$
Adiabatic Ettingshausen-Nernst coefficient	$\epsilon_{21}'=E_2^*/w_1$	$J_1=J_2=w_2=w_2^*=0$

Adiabatic condition: $w_2=0$; isothermal condition: $G_2=0$.

* This work was supported by the U. S. Army Research Office, Durham.

† Part of this work was submitted (by N. H. Z.) in partial fulfillment of the requirements for the Ph.D. degree at Louisiana State University.

[1] C. J. Bergeron, C. G. Grenier, and J. M. Reynolds, Phys. Rev. **119**, 925 (1960).

[2] H. B. Callen, Phys. Rev. **73**, 1349 (1948); **85**, 16 (1952).

[3] J. P. Jan, in *Solid State Physics*, edited by F. Seitz and D. Turnbull (Academic Press Inc., New York, 1957), Vol. 5, p. 1.

Kinetic Equations (Form I)

As usual in the thermodynamics of irreversible processes, the fluxes are written as linear functions of the affinities:

$$\mathbf{J}=\boldsymbol{\sigma}\mathbf{E}^*-\boldsymbol{\varepsilon}''\mathbf{G} \tag{1a}$$

and

$$\mathbf{w}^*=-\boldsymbol{\pi}''\mathbf{E}^*+\boldsymbol{\lambda}''\mathbf{G}. \tag{1b}$$

Here $\boldsymbol{\sigma}$ is the isothermal electric conductivity tensor; $\boldsymbol{\varepsilon}''$ is the thermoelectric power tensor; $\boldsymbol{\pi}''$ is the Peltier tensor; and $\boldsymbol{\lambda}''$ is the thermal conductivity tensor under isopotential conditions. The components of these four tensors are hereafter called the kinetic coefficients.

The quantity $\mathbf{E}^*$ is defined as the negative gradient of the electrochemical potential μ of an electron, where μ is the sum of an electrostatic component $\mu_e=-e\psi$ (ψ is the electronic charge) and a chemical component μ_c, which is a function of the temperature and the electron concentration. In terms of the free-electron theory, μ_c is the Fermi energy. $\mathbf{E}^*$ is then

$$\mathbf{E}^*=-e^{-1}\nabla(\mu_e+\mu_c)=\mathbf{E}-e^{-1}\nabla\mu_c. \tag{2}$$

The quantity $\mathbf{w}^*$ is the entropy current density times the absolute temperature:

$$\mathbf{w}^*=\mathbf{w}+e^{-1}\mu_c\mathbf{J}; \tag{3}$$

the second term above is the current density of Fermi energy.

Symmetry Relations

The system of linear equations, Eq. (1), simplifies when the current vectors are in the x_1x_2 plane and the magnetic field is in the x_3 direction, where $x_1x_2x_3$ is a Cartesian coordinate system (see Fig. 1). The transport phenomena become two dimensional and can be described in Eq. (1) by 2×2 tensors. There are then only 16 kinetic coefficients. In the case of an anisotropic medium, this reduction to two dimensions is possible if there is isotropy in the x_1x_2 plane, or if the x_3 axis is a crystalline axis of threefold, fourfold, or sixfold symmetry.

Isotropy in the x_1x_2 plane implies the symmetry relations

$$a_{ik}=(-1)^{i+k}a_{ki}, \quad (i,k=1,2) \tag{4a}$$

$$a_{11}=a_{22}, \tag{4b}$$

where a_{ik} designates an element of the 2×2 tensors defined by Eq. (1). The coincidence of the magnetic field direction with the normal to the x_1x_2 plane results in the diagonal elements of the tensors being even functions of H and the off-diagonal elements being odd functions of H:

$$a_{ik}(H)=(-1)^{i+k}a_{ik}(-H), \quad (i,k=1,2). \tag{5}$$

The symmetry relations, Eqs. (4) and (5), reduce the number of independent kinetic coefficients to eight. Each tensor is then a linear combination of the unit tensor

$$\mathbf{1}=\begin{vmatrix}1&0\\0&1\end{vmatrix}$$

and the antisymmetric tensor

$$\mathbf{i}=\begin{vmatrix}0&1\\-1&0\end{vmatrix}:$$

$$\mathfrak{a}=a_{11}\mathbf{1}+a_{12}\mathbf{i}. \tag{6}$$

Such tensors form a group isomorphic with the complex numbers $a=a_{11}+a_{12}i$ and may be manipulated in a like manner.

Onsager's Relations

The systematic application of Onsager's reciprocal relations[4] to Eq. (1) gives

$$\sigma_{ik}(H)=\sigma_{ki}(-H), \tag{7a}$$

$$\lambda_{ik}''(H)=\lambda_{ki}''(-H), \tag{7b}$$

$$T\epsilon_{ik}''(H)=\pi_{ki}''(-H). \tag{7c}$$

Equation (7c) combined with the symmetry relations gives

$$T\epsilon_{ik}''(H)=\pi_{ik}''(H),$$

or in tensor form:

$$T\boldsymbol{\varepsilon}''=\boldsymbol{\pi}''. \tag{8}$$

Relations (8) reduce the number of independent coefficients to six. In the present work, the validity of Eq. (8) was considered as one of the points to be investigated and, therefore, eight independent coefficients were determined experimentally.

Wiedemann–Franz Law

The thermal and the electrical conductivity tensors $\boldsymbol{\lambda}''$ and $\boldsymbol{\sigma}$ are not related through Onsager's relations but can be related by a generalized form of the Wiede-

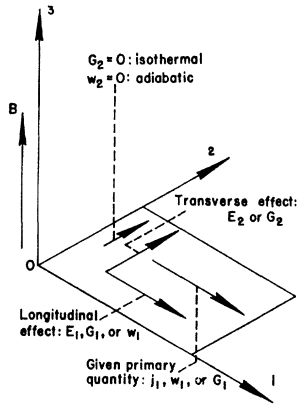

FIG. 1. A schematic representation of the fields and current quantities in a flat rectangular sample.

[4] L. Onsager, Phys. Rev. 37, 405 (1931); 38, 2265 (1931).

mann-Franz law[5] as

$$\lambda''(H)=LT\sigma(H), \tag{9}$$

where in free-electron theory L is a constant,

$$L_n=(\pi^2/3)(k/e)^2=2.45\times10^{-8}\text{V}^2/\text{deg}^2.$$

Questions arise as to the validity of Eq. (9) when the influences of anisotropy, temperature, and applied magnetic field are considered. Furthermore, these relations apply to purely electronic conduction processes and the existence of lattice conductivity in the thermal case must be either evaluated or proven negligible. Assuming all conduction processes to be purely electronic, Kohler[6] and recently Azbel, Kaganov, and Lifshitz[5] have shown that the Wiedemann-Franz law should apply to a single crystal, for arbitrary orientation and magnitude of the applied magnetic field, provided the conduction electrons are scattered without change of energy.

The effect of an applied magnetic field has been treated in the Sondheimer-Wilson model for two overlapping bands and the explicit relations calculated therefrom give the relative change of the resistivities.[7] Effective relaxation times which are different for the thermal and the electrical conductivities are assumed and the Lorenz ratio found is no longer independent of the applied magnetic field.

The system of linear equations (1) agrees in form with most of the theoretical derivations. Further, the different tensor elements are directly dependent on the number of carriers; each is a sum of the contributions of the different groups of carriers.

Kinetic Equations (Forms II and III)

Because the experimentalists usually determine resistivities, two additional approaches are taken. In the first one (Form II), the electric current density and the gradient of temperature are the independent variables

$$\text{(Form II)}\quad \begin{aligned}\mathbf{E}^*&=\boldsymbol{\rho}\mathbf{J}+\boldsymbol{\varepsilon}\mathbf{G},\\ \mathbf{w}^*&=-\boldsymbol{\pi}\mathbf{J}+\boldsymbol{\lambda}\mathbf{G},\end{aligned} \tag{10}$$

where $\boldsymbol{\rho}$ is the isothermal electrical resistivity tensor, $\boldsymbol{\varepsilon}$ is the absolute thermoelectric tensor, $\boldsymbol{\pi}$ is the isothermal Peltier tensor, and $\boldsymbol{\lambda}$ is the thermal conductivity tensor. The components of these four tensors are hereafter called the isothermal coefficients. The advantages of this formulation have been pointed out, for instance, by Mazur and Prigogine,[8] and by Callen.[9] Note that in the case of the thermoelectric and the Peltier tensors, the effects take place at the junction of two different materials. One takes care[3] of the existence of the two sides of the junction by replacing the tensors $\boldsymbol{\varepsilon}$ and $\boldsymbol{\pi}$ by $\boldsymbol{\varepsilon}_S-\boldsymbol{\varepsilon}_B$ and $\boldsymbol{\pi}_S-\boldsymbol{\pi}_B$, where $\boldsymbol{\varepsilon}_S$ and $\boldsymbol{\pi}_S$ refer to the sample and $\boldsymbol{\varepsilon}_B$ and $\boldsymbol{\pi}_B$ refer to the other side of the junction (i.e., the copper leads).

The second approach (Form III) corresponds to the conditions of measurement used in this work for the thermoelectric and the thermomagnetic effects. Two fluxes, heat current and electrical current, are imposed on the sample and the potentials and the temperature differences are measured. The appropriate kinetic equations are

$$\text{(Form III)}\quad \begin{aligned}\mathbf{E}^*&=\boldsymbol{\rho}'\mathbf{J}+\boldsymbol{\varepsilon}'\mathbf{w}^*,\\ \mathbf{G}&=\boldsymbol{\pi}'\mathbf{J}+\boldsymbol{\gamma}\mathbf{w}^*,\end{aligned} \tag{11}$$

where $\boldsymbol{\varepsilon}'$ and $\boldsymbol{\pi}'$ are the thermoelectric and the Peltier tensors, respectively, $\boldsymbol{\rho}'$ is the adiabatic electrical resistivity tensor, and $\boldsymbol{\gamma}$ is the thermal resistivity tensor. The components of these four tensors are hereafter called the adiabatic coefficients.

Simple relations exist between the different tensors defined in the foregoing. The relations used in the computations herein are, in tensor form:

$$\begin{aligned}&\boldsymbol{\sigma}=\boldsymbol{\rho}^{-1} \quad\text{and}\quad \boldsymbol{\lambda}=\boldsymbol{\gamma}^{-1} && \text{(for the conductivity tensors),}\\ &\boldsymbol{\varepsilon}=\boldsymbol{\lambda}\boldsymbol{\varepsilon}' \quad\text{and}\quad \boldsymbol{\varepsilon}''=\boldsymbol{\sigma}\boldsymbol{\varepsilon} && \text{(for the thermoelectric tensors),}\\ &\boldsymbol{\pi}=\boldsymbol{\lambda}\boldsymbol{\pi}' \quad\text{and}\quad \boldsymbol{\pi}''=\boldsymbol{\sigma}\boldsymbol{\pi} && \text{(for the Peltier tensors).}\end{aligned} \tag{12}$$

Also, the relations

$$\boldsymbol{\rho}'=\boldsymbol{\rho}+\boldsymbol{\varepsilon}\boldsymbol{\pi}' \quad\text{and}\quad \boldsymbol{\lambda}''=\boldsymbol{\lambda}+\boldsymbol{\varepsilon}\boldsymbol{\pi}'' \tag{13}$$

are occasionally useful. When any set of eight independent coefficients has been determined, any other coefficient can be calculated through the use of Eq. (12). These relations give Onsager's relations in the form

$$\boldsymbol{\pi}'=T\boldsymbol{\varepsilon}', \quad \boldsymbol{\pi}=T\boldsymbol{\varepsilon}. \tag{14}$$

Further, the Wiedemann-Franz law, Eq. (9), has the alternative forms

$$\begin{aligned}\boldsymbol{\lambda}(H)&=LT\boldsymbol{\sigma}(H),\\ \boldsymbol{\rho}(H)&=LT\boldsymbol{\gamma}(H),\end{aligned} \tag{15}$$

since the differences between elements of $\boldsymbol{\lambda}''$ and $\boldsymbol{\lambda}$ are elements of the tensor $\boldsymbol{\varepsilon}\boldsymbol{\pi}''$ and are negligible compared to the corresponding $\boldsymbol{\lambda}$ terms.

Table I shows the measured coefficients together with the conditions of measurement. As indicated in Fig. 1, the qualification "isothermal" refers to the condition $G_2=0$ and "adiabatic" refers to the condition $w_2=0$. Note that in the galvanomagnetic measurements, the more complete isothermal conditions $G_1=G_2=0$ are fulfilled.

III. APPARATUS

The electromagnet was an iron-core Weiss magnet with 8-in. pole pieces separated by a $1\frac{5}{8}$-in. airgap. It

[5] M. Ia. Azbel, M. I. Kaganov, and I. M. Lifshitz, J. Exptl. Theoret. Phys. (U.S.S.R.) **32**, 1188 (1957) [translation: Soviet Phys.—JETP **5**, 967 (1957)].
[6] M. Kohler, Ann. Physik **40**, 601 (1941).
[7] A. H. Wilson, *Theory of Metals* (Cambridge University Press, New York, 1953), 2nd ed.
[8] P. Mazur and I. Prigogine, J. Phys. Radium **12**, 616 (1951).
[9] H. B. Callen, Phys. Rev. **85**, 16 (1952).

could be rotated 360° about a vertical axis. Calibration was by means of a nuclear resonance gaussmeter.

The sample was chemically cut from a single crystal of zinc grown by a modified Bridgman method from zinc rods supplied by Johnson, Matthey, and Company. The sample dimensions were 26.58×8.10×0.345 mm. The orientation was such that when placed in the cryostat with its length along the vertical, the hexagonal axis lay in the horizontal plane at an angle of 44° with respect to the normal to the large face of the crystal.

Adiabatic conditions were obtained by placement of the sample inside a vacuum chamber[1] sealed with a gold ring.

The sample was mounted with its length parallel to the axis of the brass vacuum jacket. The upper part of the sample (Fig. 2) was clamped to a copper post extending up into the helium bath. Silicone grease was smeared between the jaws of the clamp to improve thermal contact under vacuum. A heater wound from insulated resistance (Advance No. 40) wire was placed at the opposite end of the sample. Both the current through and the voltage across the heater could be measured. The entire assembly was attached to a stainless steel pumping line, which was separated midway by an epoxy joint to provide electrical insulation for the crystal holder. The leads passed directly from the vacuum chamber into the helium bath through an epoxy seal.[10]

The temperatures at appropriate points on the crystal were measured by means of carbon-composition resistors (Allen-Bradley, 50 Ω, 1/10 W). "Matched" pairs of resistors, with closely identical behavior in the temperature range 1.3 to 4.2°K, were selected in a preliminary run. To insure good thermal contact between the resistance thermometers and the appropriate points on the crystal, a closely fitting, thin-walled, cylindrical sleeve of electrolytic copper was machined for each of the carbon resistors. A thermal lead made of No. 28 copper wire was soldered along each sleeve. The end of each thermal lead was soldered with tin solder to the desired point on the crystal. Each resistor was coated with a thin film of liquid plastic insulating compound before being placed in its copper sleeve. Each resistance thermometer had two pairs of electrical leads attached across its terminals. These leads were made of resistance wire (Advance No. 40, 32 Ω/*ft*) to minimize any instantaneous heat flow between the outside helium bath and the thermometers. Two of the thermometric probes were soldered along the direction of heat flow (separation: 1.65 cm) and the two others in the direction perpendicular to the heat flow (separation: 0.81 cm) along the edges of the sample.

The leads for electric potential measurements were soldered directly to the copper thermal leads. In this way corresponding electrical and thermometric measurements were made at exactly the same points on the sample. The electrical measuring circuit, described in reference 1, consisted of a "thermal-free" six-dial Rubicon potentiometer, a Liston-Becker dc breaker-amplifier, and a Brown recorder. A continuous signal was achieved by an increase of the magnet current at a constant rate.

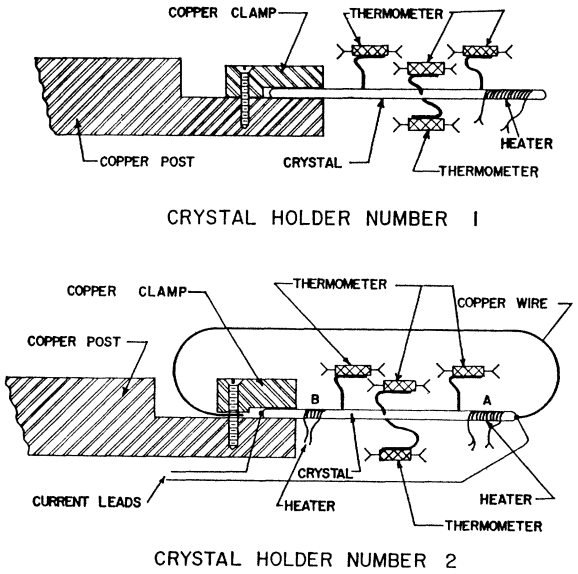

FIG. 2. The crystal holder for the measurement of the thermal magnetoresistance and the Righi-Leduc effects (number 1). The crystal holder for the measurement of the Peltier and of the Ettingshausen effects (number 2).

The temperature measuring circuit was in the form of a bridge, two arms of which were carbon-resistance thermometers. The measurement of differences of temperature ΔT of the order of magnitude of a millidegree was, thus, reduced to the measurement of the difference between the resistances of the carbon resistors. The same chain of measuring instruments used for the galvanomagnetic effects was inserted in the diagonal of the thermometric bridge circuit to provide a continuous recording of the voltage proportional to ΔT. The currents in the thermometers were chosen in the range 8 to 40 μA and held constant within 0.5% during a set of measurements.

Prior to each measurement, the bridge was balanced by adjustment of the current in one arm so that a zero signal corresponded to zero heat current and zero magnetic field for the longitudinal effects, or to zero magnetic field (with heater turned on) for the transverse effects. This procedure effectively brought the characteristic curves $R(T)$ of the pair of resistance thermometers involved into practical coincidence at the average temperature of the measurement.

A separate potentiometric circuit allowed the measurement of the resistance of each of the thermometers separately. These measurements were taken regularly during the decrease in temperature of the helium bath

[10] K. S. Balain and C. J. Bergeron, Rev. Sci. Instr. **30**, 1058 (1959).

at the start of each run and provided an accurate characteristic curve for each thermometer. The behavior of the thermometers was found to be quite reproducible, in spite of repeated cyclings from room temperature to helium temperature.

IV. RESULTS

The conditions of measurement, summarized in Table I, were chosen for the particular effects under investigation. All data were taken with the magnetic field directed along the hexagonal axis of the zinc crystal. This satisfied the necessary symmetry conditions for two-dimensional isotropy; also, the oscillatory behavior of the effects in zinc becomes negligible when the magnetic field direction is off the hexagonal axis by an angle of a few degrees. The orientation of the magnetic field was accomplished by locating the sharp relative minimum that exists in both thermal and electrical magnetoresistance.[11,12]

Bergeron, Grenier, and Reynolds[1] have shown that the departure from the ideal case of Fig. 1 because of the magnetic field making an angle of 44° with respect to the normal to the large face of the crystal is accounted for by use of an effective probe separation $d\cos 44°$ (for the transverse effects), where d is the separation of the transverse probes.

The effect due to a misalignment of the transverse probes, or that due to a misalignment of the magnetic field with the hexagonal axis, is an even function of the field. These effects are eliminated by the taking of two series of measurements with $+H$ and $-H$, respectively, and the use of their difference. The justification of the procedure for all transverse measurements is also discussed in reference 1. The misalignment of the longitudinal probes was negligible and the field reversal procedure was unnecessary for longitudinal measurements.

The Electrical and the Thermal Resistivity Tensors

The galvanomagnetic effects were measured with nearly perfect isothermal conditions, the crystal being immersed in superfluid helium. The temperature of the crystal was 2°K and the electric current in the csystal was 0.5 A.

The thermomagnetic effects were measured with the crystal inside a vacuum chamber. The chamber pressure was less than 4×10^{-6} mm of Hg, the bath temperature was 1.37°K, the mean crystal temperature was 2°K, and the heat current was 2×10^{-4} W.

The results for the thermal resistivity and the electrical resistivity are shown in Fig. 3 plotted vs the magnetic field intensity. For a check of Eq. (15), the scales have been adjusted in the ratio L_nT, where L_n is the free-electron value of the Lorenz ratio and $T=2$°K.

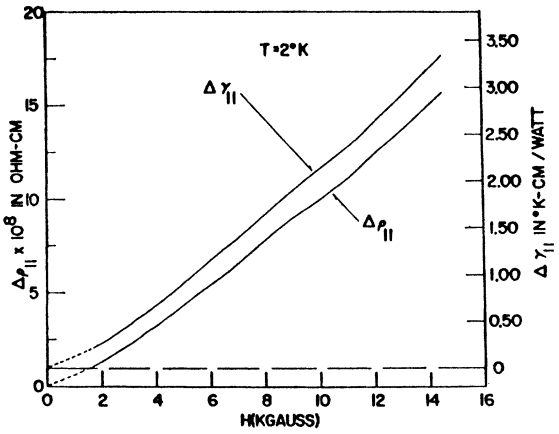

FIG. 3. The field-dependent part of the magnetoresistivity $\Delta\rho_{11}$ and the thermal magnetoresistivity $\Delta\gamma_{11}$ vs the magnetic field H at $T=2$°K. The scales have been adjusted in the ratio L_nT (L_n is the free-electron value of the Lorenz number).

The measurements gave directly the field-dependent part of the resistivities, i.e., $\gamma_{11}(H)-\gamma(0)=\Delta\gamma_{11}$ and $\rho_{11}(H)-\rho(0)=\Delta\rho_{11}$; these quantities are plotted in Fig. 3.

The zero-field electrical resistivity was determined experimentally with relatively high precision as $\rho_0=4.5\times10^{-9}$ Ω-cm at 2°K. The variation of the electrical resistivity with the field is found to be fairly linear, with $\rho(H)/\rho(0)\simeq38$ at 14 kG. This value is comparable to those of Alers[12] (Zn VI, at 3.5°K, $\rho(H)/\rho(0)\simeq10$) and Borovik[11] (Zn−10, at 4.22°K, $\rho(H)/\rho(0)\simeq33$) at the same value of the field, while for a purer crystal Renton[13] reports a much higher value (Zn−3, $\rho(H)/\rho(0)$

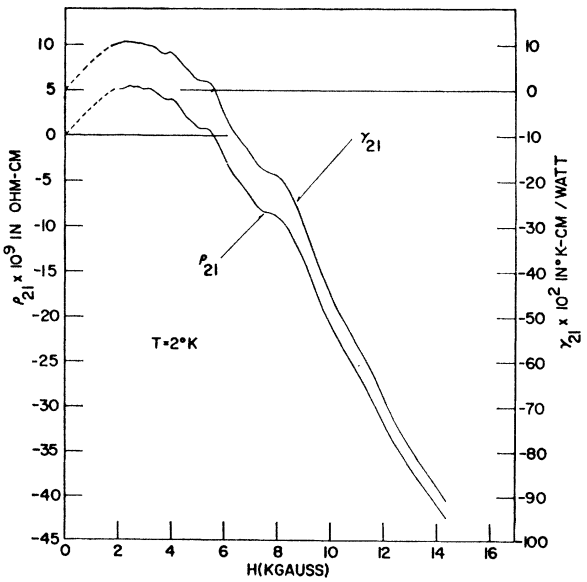

FIG. 4. The total Hall resistivity ρ_{21} and the Righi-Leduc resistivity γ_{21} vs magnetic field H at 2°K. The scales have been adjusted in the ratio L_nT.

[11] E. S. Borovik, J. Exptl. Theoret. Phys. (U.S.S.R.) **30**, 262 (1956) [translation: Soviet Phys.—JETP **3**, 243 (1956)].
[12] P. B. Alers, Phys. Rev. **101**, 41 (1956).
[13] C. A. Renton, in *Proceedings of the Seventh International Conference on Low-Temperature Physics* (University of Toronto Press, Toronto, 1960), p. 153.

$=208$ at 7 kG). The measurement of the zero-field thermal resistivity $\gamma(0)$ was, on the contrary, extremely inaccurate; it was considered preferable to compute it as $\gamma(0)=\rho(0)/L_nT$, an assumption corroborated by the results shown below. Though the presence of an oscillatory component is faintly visible, this component can be displayed unmistakably as shown in Fig. 5 of reference 1.

The results for the Hall resistivity coefficient ρ_{21} and the Righi-Leduc thermal resistivity coefficient γ_{21} are shown in Fig. 4. The oscillatory behavior superimposed on the gross variation is clearly evident in both effects. Both effects change sign for the same value of the magnetic field strength ($H=5500$ G) and the oscillations are closely in phase

Measurements were also taken at 4.2 and 3.16°K. The sensitivity of the thermometers is poorer at these temperatures. The results indicated qualitatively that the electrical magnetoresistance was practically independent of the temperature, whereas the thermal magnetoresistance varied as $1/T$, as expected from the Wiedemann-Franz law.

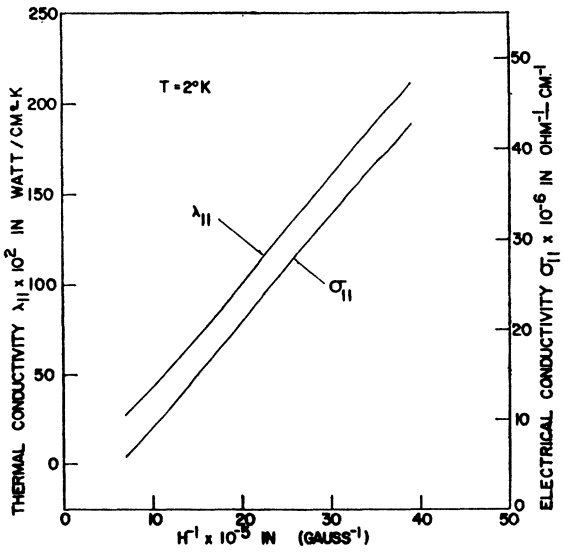

FIG. 5. The electrical and thermal conductivity coefficients σ_{11} and λ_{11} at 2°K vs the reciprocal of the magnetic field. The scales have been adjusted in the ratio L_nT.

The Electrical and the Thermal Conductivity Tensors

Knowledge of the elements of the resistivity tensors allows the elements of the conductivity tensors to be computed from the following formulas derived from Eqs. (4), (6), and (12):

$$\sigma_{ij}=\rho_{ji}/(\rho_{11}^2+\rho_{21}^2), \tag{16a}$$

$$\lambda_{ij}=\gamma_{ji}/(\gamma_{11}^2+\gamma_{21}^2), \tag{16b}$$

with $\rho_{11}=\Delta\rho_{11}+\rho_0$ and $\gamma_{11}=\Delta\gamma_{11}+\gamma_0$, where $\Delta\rho_{11}$, $\Delta\gamma_{11}$, and ρ_0 are experimentally determined while γ_0 is taken to be equal to ρ_0/L_nT.

The electrical conductivity σ_{11} and the thermal conductivity λ_{11} are shown in Fig. 5 plotted vs the reciprocal of the magnetic field. The values are plotted in the magnetic field range most favorable for the observation of oscillations. The absence of any sizable trace of oscillation in the conductivities is striking; this is discussed in Sec. V. The results for the Hall conductivity (σ_{12}) and the Righi-Leduc conductivity (λ_{12}) are shown in Fig. 6, plotted vs H. The scales have been adjusted in the ratio L_nT ($T=2$°K). These quantities go from positive to negative values near 5500 G. At high fields, the conductivities clearly go through a minimum. Their oscillations are large and in phase. In view of the strong oscillatory behavior of the Hall conductivity and its relation to the oscillation in the number of carriers, the behavior of the conductivities at very low fields was investigated to detect the presence of high-mobility carriers.

Low-field measurements were carried out for the Hall effect and the electrical magnetoresistance only, since the precision for these measurements is higher than for the thermomagnetic effects and both sets of effects are related by the Wiedemann-Franz law. These results are shown in part on the reduced scale of Fig. 6. A well-defined maximum in σ_{12} appears, located at 550 G. More detail of the lower field range is seen in Fig. 7 for the two temperatures 2 and 4.2°K. The same figure gives also the low-field values for σ_{11} at both these temperatures. These features are interpreted in terms of the Sondheimer-Wilson theory[7] in Sec. V.

The two first curves shown in Fig. 8 are plots of the purely oscillatory part of σ_{12} and λ_{12} vs the reciprocal of the magnetic field H. The scales are adjusted by the Wiedemann-Franz coefficient. It is interesting to note the close similarity between the two curves.

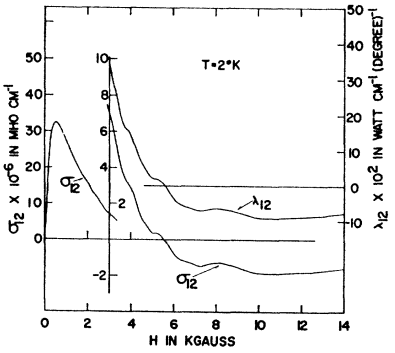

FIG. 6. The Hall conductivity σ_{12} and Righi-Leduc conductivity λ_{12} vs the magnetic field at 2°K. The scales have been adjusted in the ratio L_nT.

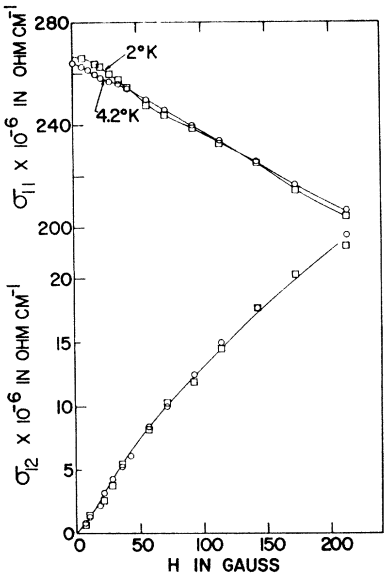

FIG. 7. The Hall conductivity σ_{12} and the magnetoconductivity σ_{11} at low fields at 4.2°K (○) and 2°K (□). The solid curve σ_{12} is calculated from a Sondheimer-Wilson four-band approximation.

The Wiedemann-Franz Law

The detailed comparison of the absolute values of thermal and electrical effects has been made in terms of the Wiedemann-Franz law. The point-by-point behavior of the Lorenz ratios $L_1=\lambda_{11}/T\sigma_{11}$ and $L_2=\lambda_{12}/T\sigma_{12}$ is shown in Fig. 9 and provide the basis for the following remarks.

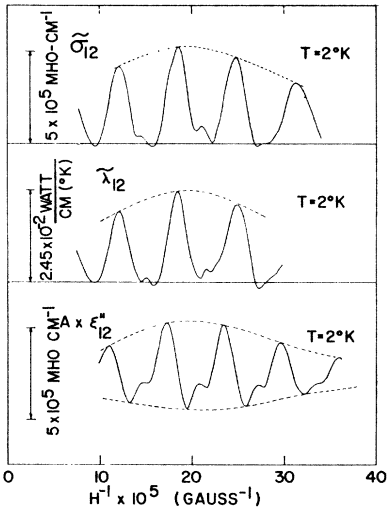

FIG. 8. Oscillation in the Hall conductivity ($\tilde{\sigma}_{12}$) and the Righi-Leduc conductivity ($\tilde{\lambda}_{12}$) vs the reciprocal of the magnetic field at 2°K. (a) The Hall conductivity oscillation $\tilde{\sigma}_{12}$ is deduced from the curve for σ_{12} in Fig. 6 using the lower envelope of the oscillations. (b) Righi-Leduc oscillations $\tilde{\lambda}_{12}$ are deduced from the λ_{12} curve in Fig. 6. The scale of this curve is adjusted through the coefficient L_nT and fits the $\tilde{\sigma}_{12}$ curve. (c) The quantity $A|\epsilon_{12}''|$ is shown in the third curve, see Eq. (43).

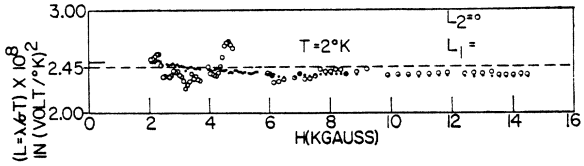

FIG. 9. The Lorenz ratios at 2°K vs the magnetic field. L_n is the Lorenz ratio for free electrons.

The "longitudinal" ratio L_1 stays within 4% of the value $L_n=2.45\times10^{-8}$ V²/deg² (the free-electron value). The "transverse" ratio L_2 stays within 6% of the same value. The region around 5.5 kG must be disregarded in the case of L_2, for both the Hall and the Righi-Leduc effects change sign and the relative errors become very large in that region. The general behaviors of L_1 and L_2 are strikingly similar. They are both larger than L_n at low fields ($H<3000$ G for L_1 and $H<2350$ G for L_2). At high fields ($H>6000$ G), they are constant and equal within the limits of experimental errors, their common value being 2.35×10^{-8} V²/deg², about 4% less than L_n. Note that the relative precision of the measurements is very high in the high-field region, where the magnitude of the effects is large.

The strong anisotropy of the magnetoresistance in zinc makes the results of the computation of the Wiedemann-Franz ratio extremely sensitive to any change (between successive runs) of the crystal orientation. The present results are from recent measurements[14] where the orientation has been carefully maintained; these recent data supersede the results reported earlier.[15] As can be seen in Fig. 8, the Wiedemann-Franz law also holds between the purely oscillatory parts of the Hall conductivity σ_{12} and the Righi-Leduc conductivity λ_{12}.

The Lattice Conductivity

The closeness of the experimental values of L_1 to that of the Lorenz number L_n indicates that the lattice thermal conductivity λ_g of the zinc sample at 2°K is small compared to the electronic conductivity λ_e. Figure 10 shows the results of two different methods used to determine the lattice thermal conductivity. One determination is based on the assumption that λ_g is independent of the magnetic field. If λ_e obeys the Wiedemann-Franz law, then $\lambda_{11}=\lambda_e+\lambda_g$ becomes

$$\lambda_{11}(H)=\sigma_{11}(H)TL_e+\lambda_g, \tag{17}$$

where L_e is a constant not necessarily equal to L_n. If L_e is independent of the magnetic field, a plot of $\lambda_{11}(H)$ vs $\sigma_{11}(H)$ is a straight line whose intersection with the vertical axis gives λ_g. It is seen in Fig. 10 that this method is appropriate and gives $\lambda_g=0.02$ W/cm-deg.

The second method depends on λ_e tending toward

[14] N. H. Zebouni, C. G. Grenier, and J. M. Reynolds, Bull. Am. Phys. Soc. 6, 10 (1961).

[15] C. J. Bergeron, C. G. Grenier, J. M. Reynolds, and N. H. Zebouni, Bull. Am. Phys. Soc. 5, 445 (1960).

zero at very large magnetic fields. The total thermal conductivity then tends towards λ_g. With an H^{-2} behavior for λ_e assumed, a plot of λ_{11} vs H^{-2} gives λ_g. This method gives $\lambda_g=0.09$ W/cm-deg. The latter estimate is not as reliable as the former because very high magnetic fields were not available. Evidently λ_g represents less than 2/1000 of the total zero-field conductivity λ_0; but at 14.2 kG, λ_g is up to about 7% of $\lambda_{11}(H)$. Alers[12] found $\lambda_g=0.5$ W/cm-deg at 3.5°K for his specimens Zn VI and Zn VII, $\lambda_g=0.2$ W/cm-deg at 3.5°K for his specimen Zn I and a still much smaller value for Zn I when the magnetic field was misaligned by 5°. The usual expression, $\lambda_g=\frac{1}{3}Cv\Lambda$, gives 0.16 W/cm-deg, where the specific heat C and the velocity of sound v are computed from a Debye temperature $\theta=308$°K and the mean free path Λ taken equal to the thickness of the crystal.

The corresponding correction to the Lorenz ratio is $(L_1-L_e)/L_1=\lambda_g/\lambda_{11}$. With the value of 0.02 W/cm-deg for λ_g, this correction is negligible at low fields but it is up to 7% at the highest field value. On the other hand, since the lattice conductivity does not contribute to the Righi-Leduc conductivity, a value of L_1 larger by 7% than L_2 should be seen in this high-field range. No such difference exists betwene L_1 and L_2. Since the precision of the measurements in the high-field range is much greater than that of the extrapolated value of λ_g, this indicates a λ_g even smaller than the value 0.02 W/cm-deg obtained from the extrapolation.

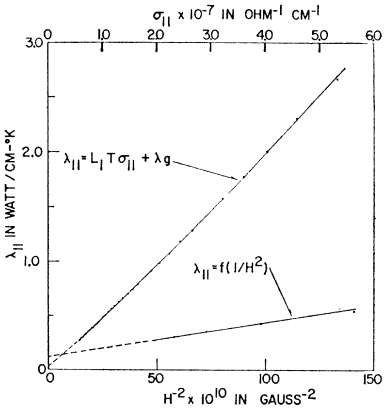

FIG. 10. The two methods of determining the value of the lattice conductivity λ_g of the zinc crystal at 2°K. In the upper curve the thermal conductivity, λ_{11} at 2°K, is plotted vs the conductivity, σ_{11}. The intercept with the λ axis gives a λ_g value of 0.02 in watt units. In the lower curve the thermal coefficient, λ_{11}, is plotted vs the reciprocal of the square of the field. Its intercept gives a λ_g value of 0.09 watt unit.

The Thermoelectric and the Ettingshausen-Nernst Effects

These effects were measured under the same conditions as the thermomagnetic effects. They were initially measured by Bergeron, Grenier, and Reynolds,[1] but a new set of measurements on the same sample was taken for use in this analysis. The experimental conditions are $J_1=J_2=J_3=0$, $w_2=0$. The kinetic equations Form III in Eq. (11) reduce to

$$\begin{aligned} E_1^* &= \epsilon_{11}' w_1^*, \\ E_2^* &= \epsilon_{21}' w_1^*, \end{aligned} \tag{18}$$

with the associated expressions for the temperature gradients $G_1=\gamma_{11}w_1^*$, $G_2=\gamma_{21}w_1^*$. The condition $\mathbf{J}=0$ gives $\mathbf{w}^*=\mathbf{w}$.

The effective fields E_1 and E_2 measured across a "thermal-free" potentiometer yield experimental coefficients $(\epsilon_{11}')_{\text{exp}}$ and $(\epsilon_{21}')_{\text{exp}}$ by

$$\begin{aligned} E_1 &= (\epsilon_{11}')_{\text{exp}} w_1, \\ E_2 &= (\epsilon_{21}')_{\text{exp}} w_1. \end{aligned} \tag{19}$$

These experimental coefficients are characteristic of the thermocouple circuit constituted by the zinc crystal and the copper leads. It can be shown that, in terms of the tensor elements of $\boldsymbol{\varepsilon}$, the thermocouple effect is characterized by the quantities $\epsilon_{11}-\epsilon_{\text{Cu}}$. Hence, from the relation $\boldsymbol{\varepsilon}'=\boldsymbol{\gamma}\boldsymbol{\varepsilon}$ the experimental relations

$$(\boldsymbol{\varepsilon}')_{\text{exp}} = \boldsymbol{\gamma}(\boldsymbol{\varepsilon}-\varepsilon_{\text{Cu}}\mathbf{1}), \tag{20}$$

or

$$\begin{aligned} (\epsilon_{11}')_{\text{exp}} &= \epsilon_{11}'-\gamma_{11}\epsilon_{\text{Cu}}, \\ (\epsilon_{21}')_{\text{exp}} &= \epsilon_{21}'-\gamma_{21}\epsilon_{\text{Cu}}, \end{aligned} \tag{21}$$

follow. The magnitude of the quantity ϵ_{Cu} was determined directly by measuring the thermocouple effect of the copper leads against superconducting lead[16] at several temperatures in the liquid-helium range. A linear dependence on the temperature was found:

$$\epsilon_{\text{Cu}} = -0.77\times10^{-2}T\ \mu\text{V/deg}.$$

This value yields terms $\gamma_{11}\epsilon_{\text{Cu}}$ and $\gamma_{21}\epsilon_{\text{Cu}}$, negligibly small compared to $(\epsilon_{11}')_{\text{exp}}$ and $(\epsilon_{21}')_{\text{exp}}$. These two quantities were then accepted without correction for the ϵ_{11}' and ϵ_{21}' coefficients.

The experimental coefficients $(\epsilon_{11}')_{\text{exp}}$ and $(\epsilon_{21}')_{\text{exp}}$ were measured at different temperatures in the liquid helium range ($1.3°\text{K}<T<4.2°\text{K}$) and found to be practically temperature independent, except for the satellite peaks which were more pronounced at the lower temperatures. The values of ϵ_{11}' shown in Fig. 11 were taken at 2.9°K and those of ϵ_{21}' shown in Fig. 12 were taken at 3°K. A change in phase of the oscillations is apparent around 4000 G, as noted previously in reference 1.

The elements of the tensors ϵ and ϵ'' appearing respectively in the kinetic equations Forms II and I were computed from Eq. (12) for comparison with theory. Figure 13 shows the behavior of the thermoelectric power ϵ_{11} and the Ettingshausen-Nernst coefficient ϵ_{21} at $T=2$°K. The latter coefficient shows a purely oscilla-

[16] F. J. Blatt and R. H. Kropschot, Phys. Rev. **118**, 480 (1960). Their extrapolated value for $\epsilon_{eu}=+0.19T\ \mu$V/deg. It is about 25 times larger than the value found in this work and of opposite sign.

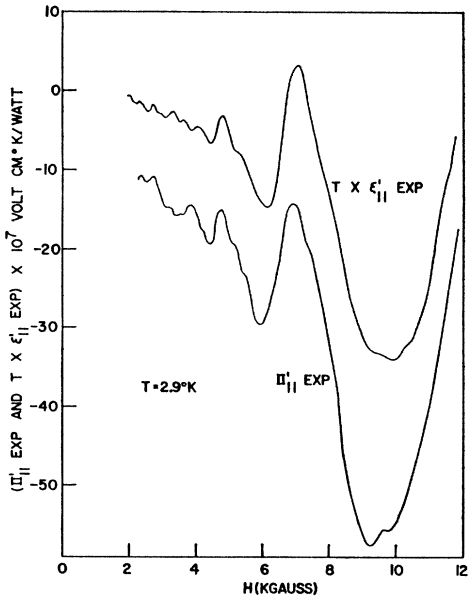

FIG. 11. The experimental thermoelectric coefficient and Peltier coefficient vs magnetic field at $T=2.9$°K. The upper curve represents the apparent adiabatic thermoelectric coefficient ϵ_{11}' multiplied by the mean temperature T of the crystal. The lower curves represent the apparent adiabatic Peltier coefficient π_{11}' at the same temperature T.

tory behavior with a set of satellite peaks. The amplitude of the oscillations shows a saturation effect. The thermoelectric power ϵ_{11} also has a marked oscillatory behavior superimposed on a small monotonic component. The principal peaks of the thermoelectric power are coincident with the satellite peaks of the Ettingshausen-Nernst coefficient. No explanation is apparent. In Fig. 14, the longitudinal kinetic coefficient ϵ_{11}'' and the transverse coefficient ϵ_{21}'' are shown as functions of H. These are the coefficients directly obtainable from standard theoretical treatments. The notable feature here is the saturation and decrease of the amplitude in the oscillations of ϵ_{21}'' at large fields. The relation to the similar behavior of the magnetic susceptibility in zinc[17] is considered in the Discussion, Sec. V.

The Peltier and the Ettingshausen Effects

The lower diagram in Fig. 2 shows the experimental arrangement for the measurement of these effects. Electric current leads of copper were soldered to each end of the zinc crystal. The measured quantities were the differences of temperature which appeared along the direction of flow of the electric current (Peltier) and transverse to it (Ettingshausen).

These measurements were expected to be extremely difficult since associated with the effects of interest are a simultaneous generation of heat by Joule's effect and a Thomson effect. A first attempt was made with the arrangement shown in Fig. 2 (crystal holder number 1) and under the same high vacuum conditions described in the section on electrical and thermal resistivity tensors. The measurements showed the existence of large thermal magnetoresistance and Righi-Leduc effects, indicating a sizable flow of heat along the crystal. To minimize any longitudinal heat flow (i.e., parallel to **J**) due to the generation of Joulean heat, a thermal junction (electrically insulated) was made between end A of the crystal and the heat sink (copper post), and an auxiliary heater was wound near end B. This arrangement is shown in Fig. 2 (crystal holder number 2). The auxiliary heater supplied a certain amount of heat to end B of the crystal; the heating was adjusted until, by reversal of the electric current, the remaining thermal magnetoresistive effect was established to be smaller than the superimposed Peltier effect. This procedure depends on the fact that the thermal magnetoresistive signal does not change sign while the Peltier effect does under electric current reversal. The experimental procedure consisted in taking the difference of two sweeps with a reversal of the electric current. Since any residual Joulean heat current is not reversed when J_1 is reversed, the difference procedure eliminates both magnetoresistance and Righi-Leduc effects. However, both Peltier and Ettingshausen effects reverse sign when the electric current is reversed and are isolated by the difference procedure. Finally, the Thomson effect, proportional to $J_1\Delta T$, is unchanged if it is associated with the reversible Peltier difference of temperature, and therefore is elimi-

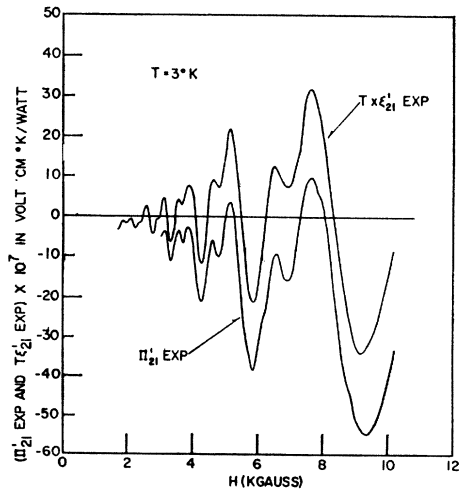

FIG. 12. The experimental Ettingshausen-Nernst coefficient and Ettingshausen coefficient at 3°K vs magnetic field. The upper curve represents the apparent adiabatic Ettingshausen-Nernst coefficient ϵ_{21}' multiplied by the mean temperature of the crystal. The lower curve represents the apparent adiabatic Ettingshausen coefficient π_{21}' at the same temperature.

[17] D. Shoenberg, in *Progress in Low Temperature Physics*, edited by C. J. Gorter (North-Holland Publishing Company, Amsterdam, 1957), Vol. II, p. 259; I. M. Dmitrenko, B. I. Verkin, and B. G. Lazarev, J. Exptl. Theoret. Phys. (U.S.S.R.) **35**, 328 (1958) [translation: Soviet Phys.—JETP **8**, 229 (1959)]; A. S. Joseph and W. L. Gordon, Phys. Rev. **126**, 489 (1962).

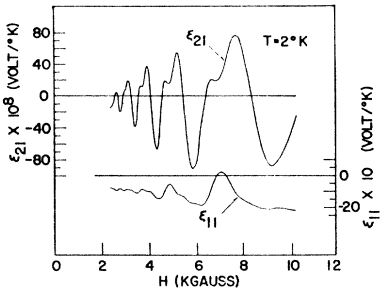

FIG. 13. The thermoelectric power and isothermal Ettingshausen-Nernst coefficient vs the magnetic field at 2°K. The lower curve is the thermoelectric power. The upper curve is the Ettingshausen-Nernst coefficient.

nated. It changes sign if it is associated with a difference of temperature due to the flow of Joulean heat. This part of the Thomson effect would not be eliminated by the current reversal procedure but is minimized by the preliminary adjustment described above.

The experimental conditions are defined by $J_2=w_2=w_2^*=0$. The definition of the Peltier coefficient $\pi_{11}'=G_1/J_1$ implies the additional condition $w_1^*=0$. This condition is experimentally satisfied to a first approximation.[18] The kinetic equation, Eq. (10), $(\mathbf{w}^*=-\boldsymbol{\pi}\mathbf{J}+\boldsymbol{\lambda}\mathbf{G})$ is now developed in the form

$$0=-(\pi_{11}-\pi_{\mathrm{Cu}})J_1+\lambda_{11}G_1-\lambda_{21}G_2,$$
$$0=-\pi_{21}J_1+\lambda_{21}G_1+\lambda_{11}G_2,$$

where, by analogy to the thermoelectric effect, a diagonal tensor[19] $\pi_{\mathrm{Cu}}\mathbf{1}$ describing the Peltier behavior of the copper leads is defined. The elements of the tensor $(\boldsymbol{\pi}')_{\mathrm{exp}}$ are experimentally determined, and the following expressions relate these experimental quantities to the associated tensors $\boldsymbol{\pi}$, $\boldsymbol{\pi}'$, and $\boldsymbol{\pi}''$:

$$\begin{aligned}\boldsymbol{\pi}&=\boldsymbol{\lambda}(\boldsymbol{\pi}')_{\mathrm{exp}}+\pi_{\mathrm{Cu}}\mathbf{1};\\ \boldsymbol{\pi}'&=(\boldsymbol{\pi}')_{\mathrm{exp}}+\boldsymbol{\gamma}\pi_{\mathrm{Cu}};\\ \boldsymbol{\pi}''&=\boldsymbol{\sigma}\boldsymbol{\lambda}(\boldsymbol{\pi}')_{\mathrm{exp}}+\boldsymbol{\sigma}\pi_{\mathrm{Cu}}.\end{aligned}\tag{22}$$

The first relation can also be written as

$$(\boldsymbol{\pi}')_{\mathrm{exp}}=\boldsymbol{\gamma}(\boldsymbol{\pi}-\pi_{\mathrm{Cu}}\mathbf{1}),\tag{23}$$

analogous to the thermoelectric relation, Eq. (20),

$$(\boldsymbol{\varepsilon}')_{\mathrm{exp}}=\boldsymbol{\gamma}(\boldsymbol{\varepsilon}-\epsilon_{\mathrm{Cu}}\mathbf{1}).$$

If the reciprocal relations Eq. (13) are assumed to apply to the zinc crystal and the copper leads (the same copper leads were used for both sets of measurements), the result is

$$(\boldsymbol{\pi}')_{\mathrm{exp}}=T(\boldsymbol{\varepsilon}')_{\mathrm{exp}}.\tag{24}$$

The elements of the Peltier tensor π_{11}' and π_{21}' were measured with the crystal at a mean temperature of 2.9 and 3°K and an electric current of 670 mA. The experimental results are shown in Figs. 11 and 12 with the corresponding experimental curve $(\epsilon_{11}')_{\mathrm{exp}}$ and $(\epsilon_{21}')_{\mathrm{exp}}$ multiplied by the above mean temperatures of 2.9 and 3°K. The phase and amplitude of the oscillations are in good agreement with Onsager's relations. The amplitudes of the longitudinal effects (Fig. 11) are matched within 5%; and those of the transverse effects (Fig. 12) are matched within 1%. The apparent discrepancy between the monotonic parts of the corresponding coefficients is probably due to a residual Thomson effect or a possible temperature drift during Peltier measurements. The monotonic variations of π_{11}' and π_{21}' are, therefore, not as reliable as those of $T\epsilon_{11}'$ and $T\epsilon_{21}'$.

V. DISCUSSION

The Long-Period de Haas–van Alphen Pockets

The pockets responsible for the long-period oscillations are probably due to a small overlap of the Fermi sphere at the lateral edge of the third Brillouin zone, this conjecture being in close agreement with the theory (single orthogonal plane wave approximation) of Harrison,[20] the effects of temperature studied by Berlincourt and Steele,[21] and the effects of low pressure[22] and high

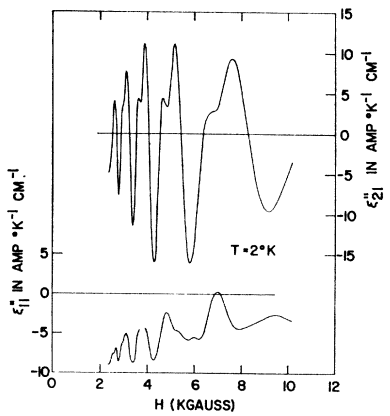

FIG. 14. The kinetic coefficients of the thermoelectric tensor at 2°K vs the magnetic field.

[18] The kinetic equation (12) describing the situation in the sample is $G_1=\pi_{11}'J_1+\gamma_{11}w_1^*$. Consider the difference of temperature $\Delta T_1=-lG_1$, where l is the length of the sample and the total currents $I_1=AJ_1$, $Q_1^*=Aw_1^*$, where A is the cross-sectional area of the sample, we have $\Delta T_1=-\Pi'I_1-\Gamma Q_1^*$ [Eq. (11)], where $\Pi'=l\pi_{11}'/A$, $\Gamma=l\gamma_{11}/A$. There exists an external thermal circuit, of equivalent thermal resistance Γ_{ext}, connecting the ends of the crystal to a heat sink (copper post in Fig. 2), and for this external circuit: $\Delta T_1=-\Gamma_{\mathrm{ext}}Q_1^*$. The comparison between the two previous equations gives $-\Pi'I_1/\Delta T_1=1-\Gamma/\Gamma_{\mathrm{ext}}$, where ΔT_1 is the quantity actually measured while $-\Pi'I_1$ is the one to be determined. But in the course of the measurements, it was estimated that each one of the thermal junctions connecting an end of the crystal to the heat sink had a thermal resistance about 150 times larger than the "internal" thermal resistance of the sample itself. It follows that Γ_{ext} is at least 300 times larger than Γ, and that, to a first approximation, $-\Delta T_1\simeq\Pi'I_1$. This is clearly equivalent to the condition $Q_1^*=w_1=0$, as shown by Eq. 11.

[19] N. H. Zebouni, Ph.D. Dissertation, Louisiana State University, 1960 (unpublished).

[20] W. A. Harrison, Phys. Rev. **118**, 1190 (1960).

[21] T. G. Berlincourt and M. C. Steele, Phys. Rev. **95**, 1421 (1954).

[22] K. S. Balain, C. G. Grenier, and J. M. Reynolds, Phys. Rev. **119**, 935 (1960).

pressure[23] on the long period of the de Haas–van Alphen type oscillation in zinc. These electron overlap regions have the shape of needle-like pockets parallel to the hexagonal axis. In a first approximation, the pockets are ellipsoidal with essentially a circular cross section in the basal plane of area in momentum space $S_m=eh/cP=1.68\times10^{-42}$ (erg-sec/cm)^2 as obtained from the experimental period of 6.28×10^{-5} G^{-1}. The ratio of the major and minor axes of the ellipsoid is taken as 16.5.[24]The number of electrons per pocket is then 1.85×10^{17} per cm^3, with the number of pockets equal to two rather than the three proposed by Verkin and Dmitrenko.[25] Hereafter, these pockets are referred to as the dHvA ellipsoids.

The Conductivities

Since the Wiedemann-Franz law is satisfied within the limits of experimental error, an analysis of the electrical conductivity is sufficient. The populations of the bands will not differ for the galvano- and thermo resistivities.[12]

With oscillations neglected, a fit to the σ_{12} curves could be sought in an expression of the Sondheimer-Wilson type.[7]

$$\sigma_{12}=(\pm)ec\sum n_iH/(H^2+H_i^2),\qquad H_i=cm_i^*/e\tau_i, \tag{25}$$

in which n_i is the number of carriers (per cm^3) in the band (+ for holes, − for electrons) and H_i is the saturation field.[26] Since such a formulation assumes quadratic energy bands, the curve fitting should not be expected to give a perfect band structure description. Harrison[20] shows clearly that the complex band structure of zinc does not satisfy the quadratic condition for which Eq. (25) is applicable.

In Fig. 7, the low-field values of σ_{12} at 4.2°K show a depression near 20 G followed by a bump near 60 G. These features may be taken as indicative of high-mobility electrons with some lower mobility holes. As seen in Fig. 6, the Hall conductivity has a maximum value of 32×10^5 mho/cm at $H=550$ G, changes sign around 5500 G, and reaches a minimum of -1.7×10^6 mho/cm around 10 000 G. This variation indicates the presence of holes with intermediate mobility and low mobility electrons. From the data at 4.2°K, the following set of characteristic values is obtained:

Carriers	n_i (cm^{-3})	H_i (G)
electron 1	1.6×10^{18}	20
holes 2	17×10^{18}	64
holes 3	2.5×10^{21}	580
electron 4	4.4×10^{21}	5150

Precision in the determination of n_1 and n_2 is poor for the following reasons: (a) The experimental precision in the low field range is relatively poor; (b) the two saturation fields are almost equal; (c) the contribution of carriers 3 and 4 is large. The 2°K data give approximately the same characteristic values for carriers 3 and 4 but a somewhat different set of values for carriers 1 and 2. There is greater uncertainty at 2°K in n_1 and n_2 because of a lower value $H_2=40$ G. The value n_1 is probably smaller than above.

A fit for the σ_{11} curve by a Sondheimer-Wilson type expression

$$\sigma_{11}=ec\sum a_in_iH_i(H^2+H_i^2), \tag{26}$$

is attempted. Here the n_i, H_i values are determined from the σ_{12} analysis. The objections which apply to fitting σ_{12} by Eq. (25) apply also to fitting σ_{11} by Eq. (26). The factor a_i is introduced in Eq. (26) to account for the existence of noncircular orbits,[27] and for the possible cases where electrons and holes of about the same cyclotron frequencies and saturation fields have compensating effects in the Hall conductivity and additive effects in the longitudinal conductivity. A strangely large value $a_1=5$ is found at 4.2°K, while at 2°K a more reasonable value closer to unity is found. The 2°K data for σ_{11} indicate a value for H_2 lower than that from the 4.2°K data and a value of a_2 of the order of 2. The 2°K data are considered more reliable than the 4.2°K data since a strong electric current through the crystal was necessary to produce sizable effects at 4.2°K and the isothermal condition was therefore more nearly achieved in the liquid-helium II bath at 2°K. For carriers 3 and 4, the values of a_i are, respectively, $a_3=2.6$ and $a_4=3.0$.

A point of interest in the zinc resistivity data which still seems obscure is the occurrence of an apparent saturation in the transverse magnetoresistance[11–13,28] under the same experimental conditions and even in the same sample[28] used in the present work. The absence of the saturation in the present results can either be attributed to some slight deterioration of the crystal or, more likely, to some misalignment of the magnetic field in the present experiment. This saturation is generally attributed to the ring-shaped hole pocket[20,29] with a very low value for the associated cyclotron frequency (very

[23] R. J. Deck, J. M. Reynolds, and C. G. Grenier, Bull. Am. Phys. Soc. **6**, 10 (1961); R. J. Deck, Ph.D. dissertation, Louisiana State University, 1961 (unpublished).

[24] A. S. Joseph, Technical Report No. 3, AFOSR-1757, Case Institute of Technology, 1961 (unpublished); also, A. S. Joseph and W. L. Gordon, Phys. Rev. **126**, 489 (1962).

[25] B. I. Verkin, I. M. Dmitrenko, Izvest. Akad. Nauk. (S.S.S.R.) Ser. Fiz. **19**, 409 (1955) [translation: Bull. Acad. Sci. (U.S.S.R.) Phys. Ser. **19**, 365 (1955).]

[26] D. E. Soule, Phys. Rev. **112**, 698 (1958).

[27] In the case the pockets present in the basal plane a symmetrical set of elliptical cross sections, the value of a is given by $a=\frac{1}{2}[(m_\alpha/m_\beta)^{1/2}+(m_\beta/m_\alpha)^{1/2}]$, where m_α and m_β refer, respectively, to extremal values of the effective mass of the electron on the ellipses; $a=1$ for energy bands of circular symmetry.

[28] S. A. Ali, Ph.D. dissertation, Louisiana State University, 1958 (unpublished).

[29] E. Fawcett, Phys. Rev. Letters **6**, 534 (1961).

TABLE II. Number of majority carriers in zinc found in the present work, compared to the two-band model data of different authors, and to the number of overlapping electrons over the boundaries of the large zone[a] taking for the crystallographic ratio[b] $c/a=1.8246$ and a single OPW approximation.

	Holes (3)	Electrons (4)
Present data		
From Hall conductivity σ_{12}	$n_3=2.5\times10^{21}$ cm^{-3}	$n_4=4.4\times10^{21}$ cm^{-3}
From conductivity σ_{11}	$a_3n_3=6.5\times10^{21}$ cm^{-3}	$a_4n_4=13.2\times10^{21}$ cm^{-3}
Alers[c] (Specimen Zn VI)		
From magnetoresistance ρ_{11}	11.2×10^{21}	17×10^{21}
From thermal magnetoresistance γ_{11}	9.14×10^{21}	22×10^{21}
Borovik[d] (Specimen Zn II)		
From Hall angle ρ_{21}/ρ_{11}	10.5×10^{21}	10.5×10^{21}
Single OPW approximation	9.1×10^{21}	9.1×10^{21}

[a] H. Jones, *The Theory of Brillouin Zones and Electronic States in Crystals* (North-Holland Publishing Company, Amsterdam, 1960), pp. 137, 192.
[b] See reference 20. [c] See reference 12. [d] See reference 11.

large saturation field). A different interpretation is suggested in the last part of the discussion. Such saturation would require the existence of a fifth carrier system with an extremely high value of the saturation field H_5; the fifth carrier system could change the above characteristic values for carriers 3 and 4. Any tilting of the magnetic field would cancel the saturation effect since most of the orbits would then be around the arms of the ring and would appear to be in the third carrier system.

The high-mobility electrons (carriers 1) as shown above probably correspond to the dHvA ellipsoids overlapping the edge of the thrid Brillouin zone even though the expected number of electrons, 0.37×10^{18} per cm^3, is smaller than the value $n_1=1.6\times10^{18}$ per cm^3 found from the curve fitting. The high-mobility holes (carriers 2) are probably part of the underlapping of the Fermi sphere in the first Brillouin zone where spin orbit splitting[30,31] is included. This underlap may be estimated to be around 1.2×10^{20} holes per cm^3 (using Joseph's[24] P_4 period and geometrical consideration of the shape of the underlap), i.e., seven times the number found in the curve fitting.

The less mobile holes characterized as carriers 3 probably consist of, partly, the less mobile holes in the above pockets in the first Brillouin zone and, mostly, the holes in the arms of the ring-shaped hole pocket in the second Brillouin zone.

The low-mobility electrons (carriers 4) correspond to the Fermi sphere overlapping in the third and fourth Brillouin zones. This overlapping is quite complex; however, the single OPW approximation gives an estimate of 9.1×10^{21} cm^{-3}, i.e., twice the value found from the σ_{12} curve fitting. The discrepancy here may arise (a) because the estimate 9.1×10^{21} cm^{-3} may be too large, or (b) because the complexity of the band structure may result in many of the electrons in the overlaps having a cyclotron mobility equal to that of some holes in the ring's arm and thus, canceling in the σ_{12} analysis. The σ_{11} curve fitting values for a_3n_3 and a_4n_4 are somewhat closer to the OPW estimate.

Several attempts have been made to compute the band structure of zinc from galvanomagnetic effects on the basis of a two-band model; these results, compared with the present data for bands 3 and 4, are shown in Table II.

The discrepancies appearing are to be expected since Eqs. (25) and (26) are only rough approximations for zinc and results depend largely on what effects are considered in the analysis. Nevertheless, results of the same order of magnitude are found here. An increase in impurities or crystal defects should cause an increase in the values for the different saturation fields and should increase the value of the field at which the Hall effect changes its sign. The present zinc crystal has shown an aging effect over a period of six years. Earlier measurements of the inversion field of the Hall effect gave successive values of 4000 G,[32] 4600 G,[1] and finally 5500 G. Also, slight increases of the residual resistance and the Dingle temperature[33] were observed. A slightly purer crystal used by Borovik[11] shows a value $H=3600$ G for the Hall inversion field. The very pure sample of Renton[13] shows a brusque appearance of the oscillation of ρ_{11} at 2000 G which suggests[1] a Hall inversion field somewhat less than 2000 G.

Oscillation in the Conductivities

The Wiedemann-Franz law also holds within the experimental error for the details in the oscillations of the galvano- and thermal conductivity tensor coefficients (Fig. 8). This behavior is expected for impurity elastic scattering,[5,7] even though to our knowledge there exists no treatment of the Wiedemann-Franz law which includes Landau quantization. Analysis of the conductivity oscillations is, therefore, restricted to the σ_{21} and σ_{11} coefficients. In reference to the oscillations, the notation $\tilde{\sigma}$ is used to represent the oscillatory part and

[30] M. H. Cohen and L. M. Falicov, Phys. Rev. Letters **5**, 544 (1960).
[31] A. S. Joseph, W. L. Gordon, J. R. Reitz, and T. G. Eck, Phys. Rev. Letters **7**, 334 (1961).
[32] C. G. Grenier, J. M. Reynolds, and S. A. Ali, *Proceedings of the Fifth International Conference on Low Temperature Physics* (University of Wisconsin Press, Madison, 1958).
[33] R. B. Dingle, Proc. Roy. Soc. (London) **A211**, 517 (1952).

$\bar{\sigma}$, the monotonic part; $\tilde{\sigma}$ represents the amplitude of the oscillation.

Levinger and Grimsal[34] showed that oscillations in the number of carriers induced by a varying magnetic field causes oscillations in the Hall constant if the remaining bands can be treated as a reservoir. Lifshitz and Kosevich[35] applied the same idea in a more comprehensive theory which treated all the isothermal coefficients of the galvanomagnetic effects. The theoretical results are summarized as follows.

The oscillatory part of the conductivity coefficients is written as

$$\tilde{\sigma}_{\alpha\beta}=\Delta\sigma_{\alpha\beta}+\Delta_1\sigma_{\alpha\beta}, \tag{27}$$

where the first term arises from the oscillation with field in the number of carriers in the different bands for the Fermi energy ζ constant, and the second term accounts for the redistribution of the carriers in the different bands due to the variation of the Fermi energy for $\sum(\pm n_i)$ constant. The first term is

$$\Delta\sigma_{\alpha\beta}=\sum_1 q_{mi}{}^{\alpha\beta}\tilde{n}_i, \tag{28}$$

where $\tilde{n}_i$ is the oscillation in the number of electrons in the pockets (i) responsible for the oscillation for $\zeta=$ const and $q_{mi}{}^{\alpha\beta}$ is the classical mobility of the carriers corresponding to the extremal cross section of the pocket perpendicular to the field. The redistribution of the carriers in the different bands yields

$$\Delta_1\sigma_{\alpha\beta}=-\sum_i\{[\sum_{i'}\bar{q}_{i'}{}^{\alpha\beta}(\partial N_i{}^0/\partial\zeta_0)+\sum_{i'}N_{i'}{}^0(\partial\bar{q}_{i'}{}^{\alpha\beta}/\partial\zeta_0)]\times[\sum_{i'}\partial N_{i'}{}^0/\partial\zeta_0]^{-1}\}\tilde{n}_i, \tag{29}$$

where the summations over i and i' are over all the bands. The index zero refers to the zero-field condition; the $q_{i'}{}^{\alpha\beta}$'s are classical mobilities; the n_i's are number of electrons or holes; and the N_i's are the number of states.

Oscillations in the Hall Conductivity

No oscillations appear in the Hall conductivity σ_{12} under asymptotic conditions, i.e., very high fields, since $q_{mi}{}^{12}=\bar{q}_i{}^{12}=\pm ec/H$. Oscillations appear only if at least one band is not under asymptotic conditions. In this case, the relaxation times are assumed to be independent of the energy and the classical mobilities are taken to be $\pm ecH/(H^2+H_i{}^2)$. Equation (27) for the Hall conductivity oscillations becomes

$$\tilde{\sigma}_{12}=ec\sum_{i,i'}H[(H^2+H_i{}^2)^{-1}-(H^2+H_{i'}{}^2)^{-1}](z_{i'}/z)(\pm\tilde{n}_i) \tag{30}$$

(+ for holes, − for electrons), where $z_{i'}=|\partial n_{i'}/\partial\zeta_{i'}|$ and $z=\sum_{i'}z_{i'}$. Since only the oscillations due to the electron ellipsoids (electrons 1) appear, the summation over i is limited to the $i=1$ term. Also, since H_1, H_2, $H_3\ll H$ (3 kG$<H<$10 kG) and z_1, z_2, $z_3\ll z$, $z_4\sim z$, the terms in $i'=1$, 2, 3 can be neglected and

$$\tilde{\sigma}_{12}=-(ec/H)[H_4{}^2/(H^2+H_4{}^2)]\tilde{n}_1. \tag{31}$$

The value $\tilde{n}$ for the oscillating number of carriers is obtained through standard methods[34–38] and, in the specific case of ellipsoids of electrons, described in connection with the long period de Haas-van Alphen pocket, is

$$\tilde{n}=4pR\hbar^{-3}\left(\frac{e\hbar H}{c}\right)^{3/2}\sum_k\frac{1}{k^{3/2}}\frac{k\lambda}{\sinh k\lambda}\times\exp\left[2\pi ik\left(\frac{cS_m}{e\hbar H}-\gamma\right)-i\left(\frac{\pi}{2}+\frac{\pi}{4}\right)\right], \tag{32}$$

where $p=2$ is the number of ellipsoids, $R=16.5$ is the ratio of the axes of the ellipsoids, and $\lambda=2\pi k^2m^*cT/e\hbar H$ is computed for $m^*=6.8\times10^{-3}m_0$ and $T=2$°K. Computation with $H_4=6250$ G limited to the fundamental terms, $k=1$, yields for the amplitude of $\tilde{\sigma}_{12}$ the values listed as a function of the field in Table III in column $|{}_1\tilde{\sigma}_{12}|$.

As evident from Table III, the experimental values $|\tilde{\sigma}_{12}|_{\rm exp}$ for the amplitudes of the σ_{12} oscillation are larger than those calculated by a factor of the order 10^4 even though they show a similar field dependence. This discrepancy might be reduced by considering larger eccentricities for the ellipsoids (R large). The limiting

TABLE III. Comparison between the amplitude of the oscillations in the experimental Hall conductivity, $|\tilde{\sigma}_{12}|_{\rm exp}$, the amplitude as computed from Lifshitz and Kosevich theory,[a] $|{}_1\tilde{\sigma}_{12}|$ [Eq. (31)], the amplitude determined from the susceptibility data,[b] $|\tilde{\sigma}_{12}|_{\rm susc}$ [Eq. (36)] and the amplitude determined from the Ettingshausen-Nernst coefficient $A|\tilde{\epsilon}_{12}''|$ [Eq. (43)] vs the magnetic field.[c]

H (kG)	$\lvert\tilde{\sigma}_{12}\rvert_{\rm exp}$ (mho cm^{-1})	$\lvert{}_1\tilde{\sigma}_{12}\rvert$ (mho cm^{-1})	$\lvert\tilde{\sigma}_{12}\rvert_{\rm susc}$ (mho cm^{-1})	$A\lvert\tilde{\epsilon}_{12}''\rvert$ (mho cm^{-1})
3	16×10^4	20.8	1.5	11×10^4
4	24×10^4	21.8	1.85	21×10^4
5	26×10^4	21.2	1.85	24×10^4
6	25×10^4	20.0	1.7	23×10^4
8	22×10^4	17.0	1.2	18×10^4
10	19×10^4	14.0	0.9	12×10^4

[a] See reference 35.
[b] See reference 25.
[c] In the different computations appearing in Tables III and IV and Fig. 8 (Curve $A\epsilon_{12}''$) the following characteristic values have been used. For the ellipsoidal pockets of electrons giving rise to the long period de Haas-van Alphen oscillations: Period $P=6.28\times10^{-5}$ G^{-1}; basal cross-section area $S_m=1.68\times10^{-42}$ erg^2 cm^{-2} sec^{+2} (or 1.51×10^{-4} A^{-2} in wave vector space); axial ratio $R=16.5$; number of electrons per pocket $n_0=1.85\times10^{17}$ cm^{-3}; number of pockets $p=2$; cyclotron mass $m^*=0.0068\,m_0$; chemical potential $\zeta_1=4.3\times10^{-14}$ erg per electron; saturation field $H_1=m^*c/e\tau_1=20$ G; relaxation time $\tau_1=2\times10^{-11}$ sec. For the low-mobility electron band: Saturation field $H_4=6250$ G, conversion units; σ in mho cm$^{-1}=(1/9)\times10^{-11}\sigma$ in Gaussian units; ϵ'' in A cm^{-1} (deg)$^{-1}=(1/3)\times10^{-9}\,\epsilon''$ in Gaussian units; λ in W cm^{-1} (deg)$^{-1}=10^{-7}\lambda$ in Gaussian units.

[34] J. S. Levinger and E. G. Grimsal, Phys. Rev. **94**, 772 (1954); E. G. Grimsal, Ph.D. dissertation, Louisiana State University, 1956 (unpublished).
[35] I. M. Lifshitz and L. M. Kosevich, J. Exptl. Theoret. Phys. (U.S.S.R.) **33**, 88 (1957) [translation: Soviet Phys.—JETP **6**, 67 (1958)].
[36] I. M. Lifshitz and L. M. Kosevich, J. Exptl. Theoret. Phys. (U.S.S.R.) **29**, 730 (1955) [translation: Soviet Phys.—JETP **2**, 636 (1956)].
[37] R. B. Dingle, Proc. Roy. Soc. (London) **A211**, 500 (1952).
[38] M. Blackman, Proc. Roy. Soc. (London) **A166**, 1 (1938).

case is that of cylindrical pockets extending to the Brillouin zone boundaries; this case gives values still only of the order 10^{-2} times the experimental values. Further, the cylinder scheme is ruled out by a vast amount of susceptibility data.[39]

In their theory, Lifshitz and Kosevich[35] express the oscillations in conductivity in terms of the oscillations in longitudinal magnetization ΔM_z. Since most susceptibility data are obtained from torsion balance experiments, a computation based on the two relations

$$n=-\partial\Omega/\partial\zeta, \tag{33}$$

$$C=-\partial\Omega/\partial\psi, \tag{34}$$

(Ω is the grand canonical potential, ζ is the chemical potential, C is the torque, and ψ is the angle between the field and the hexagonal axis) yields in the first approximation

$$\tilde{n}=\tilde{C}(\partial S_m/\partial\zeta)/(\partial S_m/\partial\psi), \tag{35}$$

$$|\tilde{\sigma}_{12}|_{\text{susc}}=Pc^2\hbar^{-1}m^*[f(\psi)]^{-1}|\tilde{C}|H^{-1}H_4^2/(H^2+H_4^2)$$
$$\simeq Pc^2\hbar^{-1}m^*H|\Delta\chi|H_4^2/(H^2+H_4^2). \tag{36}$$

Here P is the period of the oscillation in G^{-1}; $f(\psi)$, a function of ψ which can be approximated for small σ value and long ellipsoids by $f(\psi)\simeq\sin\psi\simeq\sin\psi\cos\psi$;and

$$\Delta\chi=\tilde{C}/H^2\sin\psi\cos\psi. \tag{37}$$

A better approximation is obtained by use of the exact expression for $\Delta\chi$.[40] From the data of Verkin and Dmitrenko[25] for $\Delta\chi$, the amplitudes for σ_{12} are computed and listed in Table III in the column $|\tilde{\sigma}_{12}|_{\text{susc}}$. The values $|\tilde{\sigma}_{12}|_{\text{susc}}$ and $|_1\tilde{\sigma}_{12}|$ agree within a coefficient of the order of 10; this indicates that the susceptibility oscillations in a first approximation are enhanced by oscillations in the number of electrons in the de Haas-van Alphen pocket.[37] The large discrepancy between theory and experiment exists here, too.

Calculations of $\tilde{\sigma}_{11}$ have also been made with the theory of Lifshitz and Kosevich. The expected values of $|_1\tilde{\sigma}_{11}|$ should be of the same order as $|_1\tilde{\sigma}_{12}|$, i.e., 10^{-4} times the $|\tilde{\sigma}_{12}|_{\text{exp}}$ values. The experimental data do not exhibit any detectable oscillation (i.e., $|\tilde{\sigma}_{11}|_{\text{exp}}<1\%$ of $|_1\tilde{\sigma}_{12}|$). Since an oscillation of $|\tilde{\sigma}_{11}|$ of the magnitude predicted by the Lifshitz-Kosevich theory would not be detectable in the present experiment, no contradiction to the theory exists on this point. Also, since the Lifshitz-Kosevich theory predicts the amplitude of the oscillation of σ_{11} and σ_{12} in bismuth quite well,[41] the large oscillation of $|\tilde{\sigma}_{12}|$ in zinc is not construed as contradictory to the theory. Instead, a mechanism is suggested later in the discussion which can account for this discrepancy.

[39] D. Shoenberg, in *Progress in Low Temperature Physics* (North-Holland Publishing Company, Amsterdam, 1957), Vol. II, p. 226 (a list of 12 references can be found in this review article).

[40] B. Lax, Rev. Mod. Phys. **30**, 122 (1958).

[41] J. R. Sybert, Ph.D. dissertation, Louisiana State University 1961 (unpublished).

The Wiedemann-Franz Law

As pointed out already, the oscillatory parts of the thermal and the electrical conductivity coefficients are in good agreement with the generalized Wiedemann-Franz law, $\lambda=LT\sigma$, and the coefficient L is nearly equal to the Lorenz number $L_n=(\pi^2/3)(k/e)^2$.

It has been shown through Eq. (30) that the electrons responsible for the oscillations in σ_{12} are mostly the electrons in the dHvA pocket, heretofore called electrons 1, i.e., electrons of effective mass $m_1^*=0.0068\,m_0$.The question of the effect of electron-electron Coulomb interaction on the de Haas–van Alphen effect and on transport properties such as dc conductivity has been discussed recently.[42] Diverging points of view have been expressed. Pippard has suggested that the above equation for L_n should involve the effective charge e^* rather than the bare charge e. Stern's theory (in the absence of electron-phonon interactions) predicts $e^*=em^*/m$, which, in the case of the dHvA pocket in zinc, would lead to $e_1^*=0.0068e$ and, consequently, a value of L_1 (pertaining to electrons 1) much larger than L_n. Either the Stern theory is in error, or the majority of the electrons participating in the oscillation of the conductivities have $m^*\approx m_0$. A mechanism proposed in the last part of the discussion to account for the large oscillation in the Hall conductivity gives $m^*\approx m_0$ for the contributing electrons.

The Thermoelectric Effects

Onsager's relations hold for the amplitude of the oscillations. The discrepancy between the monotonic parts of the ε' and π' is probably due to a systematic experimental error, the source of which has not yet been found. The ϵ' part is probably the most accurate. In the computation of the elements of the ϵ'' tensor, any inaccuracy introduces the same order of inaccuracy in the monotonic part of ϵ_{11}''. Since an accurate determination of the monotonic part of either ϵ_{12}'' or ϵ_{11}'' is quite difficult, no analysis has been attempted. Under asymptotic conditions in the quadratic bands model, the coefficient $\epsilon_{21}''=\frac{1}{2}cC/H$, where C is the electronic specific heat; nonasymptotic conditions lead to a somewhat smaller value. For an average value[43] for C of $595T$ erg/cm²-deg, $H=5000$ G, and $T=2°$K, ϵ_{21}'' is calculated to be 1.19 A/cm-deg or 8% of the experimental amplitude. Because of the complex harmonic content in the ϵ_{21}'' data, the existence of a monotonic part of this magnitude is difficult to ascertain.

[42] See papers by L. M. Falicov on the velocity and effective charge of the particles near the Fermi surface, by E. A. Stern on the effect of interactions on determination of Fermi surfaces, and discussion, p. 67ff, in *The Fermi Surface*, edited by W. A. Harrison and M. B. Webb (John Wiley & Sons, New York, 1960).

[43] J. G. Daunt, in *Progress in Low Temperature Physics*, edited by C. J. Gorter (North-Holland Publishing Company, Amsterdam, 1957), Vol. I, p. 202 (J. G. Daunt gives table and reference of different experimental determinations of C for zinc).

The Oscillations in the Thermoelectric Effects

No complete theory for the oscillations in the thermoelectric effects is available. There exist some indications that classical formulae[44] can be carried over to quantum theory. This procedure leads to an oscillatory term in ϵ_{21}'' related to the oscillation in the density of states as, asymptotically,

$$\tilde{\epsilon}_{12}''=\tfrac{1}{3}\pi^2k^2cT\sum_i|\partial N_i/\partial\zeta|H^{-1}, \quad (38)$$

where the oscillations appear through $\partial N_i/\partial\zeta$. Since only the oscillations due to the electron ellipsoids (electrons 1) appear, Eq. (38) reduces to

$$\tilde{\epsilon}_{21}''=\tfrac{1}{3}\pi^2k^2cT(\partial\tilde{n}/\partial\zeta)H^{-1}, \quad (39)$$

where $\tilde{n}$ without index corresponds to the dHvA pockets, Eq. (32). (Asymptotic conditions are certainly obtained for this case.)

Equation (32) for $\tilde{n}$ depends on ζ through the amplitude term and the phase. In $\partial\tilde{n}/\partial\zeta$, the most important term arises from the derivative of the phase (S_m depends on ζ)

$$\frac{\partial\tilde{n}}{\partial\zeta}=4pR\hbar^{-3}\left(\frac{e\hbar H}{c}\right)^{3/2}\frac{2\pi c}{ehH}\frac{\partial S_m}{\partial\zeta}\sum_k\frac{1}{k^{1/2}}\frac{k\lambda}{\sinh k\lambda}\times\exp\left\{2\pi ik\left(\frac{c}{ehH}S_m-\gamma\right)-i\frac{\pi}{4}\right\}. \quad (40)$$

Greater harmonic content in the $\tilde{\epsilon}_{21}''$ than in $\tilde{\sigma}_{21}$ is expected as seen by comparison of Eqs. (32) and (40). The difference in phase between the two effects of $\pi/2$ is also expected. These expectations are born out in Fig. 8 as can be seen by comparison of the first and third curves.

The amplitude of the oscillations $|\tilde{\epsilon}_{21}''|$ are computed for $T=2°\text{K}$, $(\partial S_m/\partial\zeta)=2\pi m^*$, $m^*=0.0068m_0$, and the fundamental term $k=1$ only. For these calculations, Eq. (39) is written as

$${}_1\tilde{\epsilon}_{12}''=\frac{pR(2\pi)^3c^2}{3ehH^2}\left(\frac{eH}{c\hbar}\right)^{3/2}\frac{\partial S_m}{\partial\zeta}\frac{k^2\lambda T}{\sinh\lambda}\times\sin\left\{\frac{cS_m}{ehH}-2\pi\gamma+\frac{\pi}{4}\right\}. \quad (41)$$

The computed values are shown in Table IV in the column $|{}_1\tilde{\epsilon}_{21}''|$. Again, a great discrepancy between theory and experiment is found, the ratio of calculated to experimental values being approximately 10^{-4}. The field dependences match relatively well.

A direct relation between $|{}_1\tilde{\sigma}_{12}|$ and $|{}_1\tilde{\epsilon}_{12}''|$ is found from Eqs. (31), (32), (39), and (40) as approximately,

$$|{}_1\tilde{\epsilon}_{12}''|=\frac{4\pi^4k^2cm^*T}{3e^2hH}\left(1+\frac{H^2}{H_4^2}\right)|{}_1\tilde{\sigma}_{12}|. \quad (42)$$

Substitution of $|\tilde{\sigma}_{12}|_{\text{exp}}$ for $|{}_1\tilde{\sigma}_{12}|$ in Eq. (42) gives a value for $|\tilde{\epsilon}_{12}''|$ which should be correlated with $|\tilde{\epsilon}_{12}''|_{\text{exp}}$. Equation (42) can be inverted to give a value for $|\tilde{\sigma}_{12}|$ in terms of $|\tilde{\epsilon}_{12}''|_{\text{exp}}$ as

$$|\tilde{\sigma}_{12}|\approx\frac{3e^2hH_4}{4\pi^4k^2cm^*T}\left(\frac{H}{H_4}+\frac{H_4}{H}\right)^{-1}|\tilde{\epsilon}_{12}''|_{\text{exp}}=A|\tilde{\epsilon}_{12}''|_{\text{exp}}. \quad (43)$$

Comparison of the first and third curves in Fig. 8 shows a close correlation between the two when H_4 is taken to be 6250 G. This value of H_4 is close to the 5200 G obtained from the Sondheimer-Wilson curve fitting. The values of $A|\tilde{\epsilon}_{12}''|$ are also listed in Table III. Good correlation exists between ϵ_{12}'' and σ_{12}; however, both the Lifshitz-Kosevich theory for σ_{21} and the density of state formulation for ϵ_{21}'' fail to give the right order of magnitude for the amplitude of the oscillations in zinc. In the field range studied, $3000\text{ G}<H<10\,000\text{ G}$, the factor A is practically constant, hence, the close similarity between the σ_{12} and ϵ_{12}'' oscillations. As pointed out earlier, the Lifshitz-Kosevich theory predicts quite well the oscillatory behavior of both σ_{12} and σ_{11} in bismuth. Also,[41] good agreement exists in bismuth for the oscillatory behavior of ϵ_{12}'' for the density of state formulation as above.

A direct relation between ϵ_{12}'' and $\Delta\chi$ is obtained from Eqs. (36) and (43) under the same assumption as above. Except for a difference in phase and harmonic content, the relation is

$$|\tilde{\epsilon}_{12}''|_{\text{susc}}=\tfrac{2}{3}\pi^3k^2c^3(eh)^{-2}PT(m^*)^2|\Delta\chi|. \quad (44)$$

This expression shows a field-independent proportionality between ϵ_{12}'' and $\Delta\chi$. But as shown in Table IV, these quantities differ by the same order of magnitude as found in Table III between $|\tilde{\sigma}_{12}|_{\text{susc}}$ and $|\tilde{\sigma}_{12}|_{\text{exp}}$.

TABLE IV. Comparison between the amplitude of the oscillation in the experimental Ettingshausen-Nernst kinetic coefficient $|\epsilon_{12}''|_{\text{exp}}$, the amplitude as computed from the density of state $|{}_1\epsilon_{12}''|$ [Eq. (41)], the amplitude as determined from the susceptibility[a] $|{}_1\epsilon_{12}''|_{\text{susc}}$ [Eq. (44)] vs magnetic field.

H (kG)	$\lvert\tilde{\epsilon}_{12}''\rvert_{\text{exp}}$ [A cm^{-1} (°K)$^{-1}$]	$\lvert{}_1\tilde{\epsilon}_{12}''\rvert$ [A cm^{-1} (°K)$^{-1}$]	$\lvert{}_1\tilde{\epsilon}_{12}''\rvert_{\text{susc}}$ [A cm^{-1} (°K)$^{-1}$]
3	8.15	16×10^{-4}	11.3×10^{-5}
4	13.3	14.2×10^{-4}	11.8×10^{-5}
5	14.2	13×10^{-4}	11×10^{-5}
6	13.2	12×10^{-4}	10×10^{-5}
8	10.5	10.5×10^{-4}	7.2×10^{-5}
10	7.7	9.4×10^{-4}	5.6×10^{-5}

[a] See reference 25.

[44] Y. A. Bychkov, L. E. Gurevich, and G. M. Nedlin, J. Exptl. Theoret. Phys. (U.S.S.R.) **37**, 534 (1959) [translation Soviet Phys.—JETP **10**, 377 (1960)].

The case for the oscillation in ϵ_{11}'' in zinc is questionable since the small oscillations found in the computation of ϵ_{11}'' from the experimental ε', ϱ, and γ could be due to accumulated experimental errors. For example, in calculations for ϵ_{11}'', there exist two strongly oscillatory terms which almost cancel each other. An error of 10% in either of these terms could cause the ϵ_{11}'' oscillations shown in Fig. 14. Consequently, no analysis is made for this coefficient. The Zil'berman theory,[45] which considers only σ_{11} and ϵ_{11}'' could not be compared with experiment for the same reason.

Holes and Electrons Orbits in Zinc

The anomalously large amplitude of the oscillations in the Hall conductivity is puzzling. All present theories predict an asymptotic behavior given by the general formula $\sigma_{12}=ec\sum_i(\pm n_i)/H$ (with $-$ for electrons, $+$ for holes). Since $\sum_i(\pm n_i)=0$ is expected in zinc, σ_{12} should vanish at high fields with zero oscillations. Nonvanishing Hall conductivity and oscillatory behavior would appear only if some bands do not satisfy the asymptotic conditions or if $\sum_i(\pm n_i)=n\neq 0$. In the latter case, the asymptotic expression for a change in conductivity $\Delta\sigma_{12}$ associated with a change Δn in $\sum_i(\pm n_i)$ is $\Delta\sigma_{12}=ec\Delta n/H$. To match $\Delta\sigma_{12}$ with the observed amplitude of the oscillation, the corresponding Δn must be nearly 280 times the number of electrons in the dHvA pocket. On the other hand, if the condition $\sum_i(\pm n_i)=0$ is fulfilled under nonasymptotic conditions, an equal variation in the number of holes and electrons is required ($\Delta n_h=\Delta n_e$) and the value of Δn_e will still be larger than the Δn found in the preceding consideration, i.e., of the order of 10^3 times the number of electrons in the dHvA pockets.

A special mechanism is needed which will allow many more electrons to participate than are normally expected for standard processes. A mechanism is suggested which will allow carriers normally behaving as holes to shift into electron-behaving carriers as the field is increased. In the single OPW approximation for zinc, the basal representation of which is shown in Fig. 15, an electron under the influence of the magnetic field (perpendicular to the basal plane) moves in momentum space along arc A of the Fermi sphere. Should the periodic lattice potential associated with the Brillouin planes P and P' be zero, the electron would continue along the Fermi sphere from A to C and behave as an electron carrier. For a nonvanishing potential, Bragg reflection occurs on P' and in the momentum representation, the electron passes from A to B' or, in the cellular representation, from A to B and continues along the external cross section of the hole ring,[20,29] behaving as a hole carrier. The periodic potential corresponding to the set P, P' is known to be small and to give a small energy gap which almost vanishes on the edge Q of the zone, the intersect

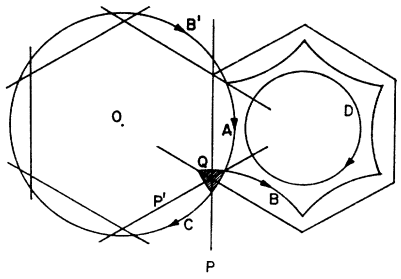

FIG. 15. The Fermi surface for Zn in an extended zone scheme (folded and unfolded Fermi surface) according to a single OPW approximation. The de Haas–van Alphen pocket is in solid black.

of P, P'.[46] An intermediate case with partial Bragg reflection may occur, with the probability of Bragg reflection decreasing as point Q is approached and as the magnetic field increases. Electrons in the second zone in momentum space passing from A to C tunnel through the edge of the third zone which contains the electron ellipsoids. As the transit electrons (i.e., the electrons bridging from A to C) are for a short while with momenta and energy closely equal to those of the electrons belonging to the de Haas–van Alphen ellipsoids, a strong interaction is expected, making the transit electrons sensitive to the Landau levels of the de Haas–van Alphen ellipsoids. This might be expected to give rise to a Bragg reflection deficiency or transparency with an oscillatory character of a period determined by the Landau levels in the small pocket.

If an amount Δn_h of carriers with an $A\rightarrow B$ hole behavior shifts to an $A\rightarrow C$ electron behavior because of the appearance of a transparency, the condition $\sum_i(\pm n_i)=0$ becomes $\sum_i(\pm n_i)=-2\Delta n_h$ with an asymptotic contribution to the Hall conductivity $\sigma_{12}=-2ec\Delta n_h/H$, and a negligible contribution to the conductivity $\sigma_{11}=q_e\Delta n_e-q_h\Delta n_h$ (with $\Delta n_e=\Delta n_h$ and mobilities $q_e\approx q_h$). From the idea of an oscillatory field dependence of the transparency, oscillation in σ_{12} related to the $\tilde{\Delta}n_h$ is expected with practically no oscillatory contribution in the σ_{11}. If the number $\tilde{\Delta}n_h$ were large enough, the experimental behavior could be explained by such a mechanism. The mechanism of magnetic breakdown invoked by Cohen and Falicov[47] to explain the giant orbit in magnesium is somewhat similar to the above mechanism except that the breakdown condition $\hbar\omega\approx\Delta A$, where ΔA is the energy gap, seems to lead to a rather different representation of the transit electrons.[48]

[45] G. E. Zil'berman, J. Exptl. Theoret. Phys. (U.S.S.R.) **29**, 762 (1955) [translation: Soviet Phys.—JETP **2**, 650 (1956)].

[46] H. Jones, *The Theory of Brillouin Zones and Electronic States in Crystals* (North-Holland Publishing Company, Amsterdam, 1960), p. 191.

[47] M. H. Cohen and L. M. Falicov, Phys. Rev. Letters **7**, 231 (1961).

[48] If the probability of crossing the set P, P' should be taken as the square of probability for the crossing of a single plane P under the breakdown condition, a practically negligible effect of transparency will take place at the field used. More probably the set, P, P', should be treated as a whole and the transition of the electrons from band 2 to band 2 as a tunneling through band 3 instead of a band 2 to band 3 transition followed by an independent band 3 to band 2 transition.

The maximum number $\Delta_{max}n_h$ of low-field $A \rightarrow B$ hole-behaving carriers which can shift to a high-field $A \rightarrow C$ electron behavior will probably correspond to that outer ring of the Fermi sphere whose inner limit is the cylinder of radius OQ passing through the edge of the zone. An approximate computation gives $\Delta_{max}n_h \approx 2\times10^{20}$ electron/cm^3, which is about 600 times the number of electrons in the de Haas–van Alphen ellipsoids, and about 3 times as much as the number needed to account for the oscillations observed in σ_{12}. Where the $A \rightarrow C$ behavior is complete, the expectation is that $\sum_i(\pm n_i) = -2\Delta n_h = -4\times10^{20}$ cm^{-3}. This amount is about 5 times smaller than the value $n_3 - n_4 = -19\times10^{20}$ cm^{-3} obtained from the σ_{12} Sondheimer-Wilson curve fitting.

Questions still exist as to how to interpret the transport properties of a ring-shaped band.[29] The electrons corresponding to the inner cross sections of the hole ring (orbit D) should be electrons in character if they were not constrained by the hole-behaving outer cross section. If the outer part of the ring is allowed to have an electron behavior, then the inner part will exhibit its electron character and the value $n_3 - n_4$ found experimentally would be quite reasonable. Also, an enhancement of the oscillation amplitude might be expected.

The condition $\sum_i(\pm n_i) \neq 0$ explains also the saturation found for the transverse magnetoresistance ρ_{11} with the magnetic field perpendicular to the basal plane, Because of the thinness of the core of the hole ring, an angle ψ of the magnetic field with respect to the normal to the basal plane increased above 5 to 10° would cause all the possible oribts related to the hole ring to be around the arms of the ring and thus give a hole character to the entire hole ring. The condition $\sum_i(\pm n_i) = 0$ would then be fulfilled and the quadratic behavior of the magnetoresistance restored at such field orientations. It is interesting to note that the oscillations in the galvanomagnetic effects disappear for such orientations.

Another feature of the mechanism is that it can explain the puzzling properties of the susceptibility oscillations in zinc, i.e., the decrease of their amplitude as the field is increased. If more electrons pass through band 3, either a larger broadening or a decrease in occupancy of the Landau levels in this band would be expected and would cause a susceptibility amplitude decrease.

The consequences of such a mechanism on the behavior of the Ettingshausen-Nernst and the thermoelectric effects are not clear at present. An enhancement of the effects would reasonably be expected. Why a phase difference of $\pi/2$ should exist between the $\tilde{\epsilon}_{12}''$ and $\tilde{\sigma}_{12}$ and also why these two effects correlate so well by means of Eq. (43) are puzzles for later unraveling.

VI. CONCLUSIONS

Some of the conclusions which can be drawn from the experimental results on electron transport phenomena in zinc are the following:

(I) The Wiedemann-Franz law holds even in the details of the oscillations of the different conductivity coefficients. This is in good agreement with the general considerations of elastic scattering by impurities at low temperature and demonstrates the relatively negligible contribution of the lattice to the heat conductivity.

(II) Onsager's relations hold in the very details of the oscillations in the thermoelectric and the Peltier tensor coefficients, in agreement with the universal validity of these relations. No Umkehr effect was detected in the oscillatory components.

(III) Interpretation of the amplitude of the oscillations in the transport phenomena in terms of oscillations in the number of carriers and the density of states leads to a strong disagreement with experiment in the case of the Hall conductivity σ_{12} and the Ettingshausen-Nernst coefficient ϵ_{21}'', but leads to fairly good agreement with the susceptibility and the conductivity term σ_{11}. A mechanism is suggested which strongly enhances the oscillations in the Hall conductivity and in the Ettingshausen-Nernst effect without affecting appreciably the susceptibility and the conductivity σ_{11}.

The theoretical implications of the foregoing conclusion are particularly interesting. It is expected that these matters will be treated at a later date. The interesting effects found in zinc are being sought in other metals.

ACKNOWLEDGMENT

The authors wish to thank Dr. C. J. Bergeron for his assistance in the early part of this work.